

A glucose biosensor based on novel Lutetium bis-phthalocyanine incorporated silica-polyaniline conducting nanobeads

AL-SAGUR, H., KOMATHI, S., KARAKAŞ, H., ATILLA, D., GÜREK, A.G., BASOVA, T., FARMİLO, Nick <<http://orcid.org/0000-0001-5311-590X>> and HASSAN, Aseel <<http://orcid.org/0000-0002-7891-8087>>

Available from Sheffield Hallam University Research Archive (SHURA) at:

<https://shura.shu.ac.uk/17705/>

This document is the Accepted Version [AM]

Citation:

AL-SAGUR, H., KOMATHI, S., KARAKAŞ, H., ATILLA, D., GÜREK, A.G., BASOVA, T., FARMİLO, Nick and HASSAN, Aseel (2018). A glucose biosensor based on novel Lutetium bis-phthalocyanine incorporated silica-polyaniline conducting nanobeads. *Biosensors & bioelectronics*, 102, 637-645. [Article]

Copyright and re-use policy

See <http://shura.shu.ac.uk/information.html>

A glucose biosensor based on novel Lutetium bis-phthalocyanine incorporated silica-polyaniline conducting nanobeads

H. Al-Sagur¹, S. Komathi¹, H. Karakaş², D. Atilla², A. G. Gürek², T. Basova^{3,4}, N. Farmilo¹
and A. K. Hassan^{1*}

¹*Materials and Engineering Research Institute, Sheffield Hallam University, Sheffield, UK*

²*Gebze Technical University, Department of Chemistry, Gebze 41400, Kocaeli, Turkey*

³*Nikolaev Institutes of Inorganic Chemistry SB RAS, Lavrentiev Pr. 3, Novosibirsk 630090, Russia*

⁴*Novosibirsk State University, Pirogova Str. 2, Russia*

** Corresponding author*

Abstract

The facile preparation of highly sensitive electrochemical bioprobe based on lutetium phthalocyanine incorporated silica nanoparticles ($\text{SiO}_2(\text{LuPc}_2)$) grafted with Poly(vinyl alcohol-vinyl acetate) itaconic acid (PANI(PVIA)) doped polyaniline conducting nanobeads ($\text{SiO}_2(\text{LuPc}_2)\text{PANI(PVIA)-CNB}$) is reported. The preparation of CNB involves two stages (i) pristine synthesis of LuPc_2 incorporated SiO_2 and PANI(PVIA); (ii) covalent grafting of PANI(PVIA) onto the surface of $\text{SiO}_2(\text{LuPc}_2)$. The morphology and other physico-chemical characteristics of CNB were investigated. The scanning electron microscopy images show that the average particle size of $\text{SiO}_2(\text{LuPc}_2)\text{PANI(PVIA)-CNB}$ was between 180-220 nm. The amperometric measurements showed that the fabricated $\text{SiO}_2(\text{LuPc}_2)\text{PANI(PVIA)-CNB/GOx}$ biosensor exhibited wide linear range (1-16 mM) detection of glucose with a low detection limit of 0.1 mM. $\text{SiO}_2(\text{LuPc}_2)\text{PANI(PVIA)-CNB/GOx}$ biosensor exhibited high sensitivity ($38.53 \mu\text{A mM}^{-1} \text{cm}^{-2}$) towards the detection of glucose under optimized conditions. Besides, the real (juice and serum) sample analysis based on a standard addition method and direct detection method showed high precision for measuring glucose at $\text{SiO}_2(\text{LuPc}_2)\text{PANI(PVIA)-CNB/GOx}$ biosensor. The $\text{SiO}_2(\text{LuPc}_2)\text{PANI(PVIA)-CNB/GOx}$ biosensor stored under refrigerated condition over a period of 45 days retains ~ 96.4 % glucose response current.

Key words: Silica nanoparticles, conducting nanobeads, lutetium phthalocyanine, glucose biosensor, PANI(PVIA)

1. Introduction

Diabetes mellitus is a major public health problem, accounting 246 million people worldwide (Tabish, 2007). The human body tightly regulates glucose levels, however, abnormalities in blood sugar levels hyperglycemia (high) or hypoglycemia (low) result in serious, potentially life-threatening complications (Peters et al., 2015). The predictions show that the rate of diabetic people will increase by about 58% by 2025 (380 million) and it is the fourth prevalent cause of death (International Diabetes Federation, 2006; Tirimacco et al., 2010). Factors that limit hospitalisations of diabetic patients include regular/continuous monitoring and control of the glucose level in the body (Shafiee et al., 2012). A variety of unambiguous methods for detecting and quantifying glucose in assorted biological fluids and food matrices exist which include spectrophotometric, calorimetric, chromatographic and electrochemical approaches. Electrochemical biosensors have gained immense acceptance in the field of medical diagnostics due to their attributes of simple, real-time, rapid and economical systems. The device comprises of a synergistic combination of biological recognition element (biotechnology) and a compatible transducer (microelectronics) (Singh et al., 2009). Glucose oxidase (GOx from *Aspergillus niger*) is a homodimer enzyme, which contains one iron atom and one flavin adenosine dinucleotide cofactor which catalyzes the conversion of β -d-glucose to d-glucono-1,5-lactone (Galant et al., 2015). GOx has been widely used in the determination of glucose for its excellent specificity to the analyte and catalyzing activity (Piao et al., 2015; Zebda et al., 2011).

Nevertheless, the major challenges in the development of GOx based amperometric biosensors are (i) higher loading of enzyme (sensitivity), (ii) stability of immobilized enzyme, and (iii) reduction in high overpotentials (Singh et al., 2009). Hence the host matrix and the immobilization strategy employed synergistically influence the performance of the biosensors (Li et al., 2000). Several electrodes modifying materials such as carbon based nanomaterials, polymers, metal nanoparticles and silica nanostructures or their hybrids have been widely used for GOx immobilization (Zhu et al., 2014). Among them silica being inert, non-toxic, with tunable porosity and inexpensive to synthesize will suit for this potential application (He et al., 2010; Y. Zhao et al., 2009). Further, silica imparts biocompatibility and hydrophilicity for the immobilized enzyme as well as prevents enzyme leakage (Jaganathan and Godin, 2012). However, mere higher loading of GOx alone is not enough; the immobilized enzyme needs to show higher activity too. The relatively poor conductivity of pristine silica makes it difficult to use in practical electrochemical biosensor application (Fang et al., 2015).

Phthalocyanines (Pcs) are planar 18 π -electron aromatic compounds with a considerably large π -delocalized surface; they are promising functional materials for diverse applications (Binnemans, 2005). Owing to their excellent electronic properties, rich redox chemistry and high physico-electrochemical stability metal Pc (MPcs) derivatives are widely employed as molecular wires in biosensor applications (Cui et al., 2015; Mani et al., 2014). Nanocomposites of d-block (Co, Cu and Zn) Pcs incorporated graphene/carbon nanotubes has been employed for amperometric glucose biosensor construction (Zhang et al., 2013; Wang et al., 2015; Cui et al., 2013; Devasenathipathy et al., 2015). Olgac et al. reported ZnPc mediated detection of glucose in real samples (Olgac et al., 2017). Double decker lutetium phthalocyanine (LuPc₂) in particular is attractive due to its high intrinsic conductivity redox properties, and chemical stability compared to several other MPcs (Basova et al., 2008a; Basova et al., 2008b). Recently Al-Sagur and coworkers reported on glucose biosensor construction using LuPc₂ as redox mediator decorated in conducting polymer hydrogel (Al-Sagur et al., 2017). Thin films of LuPc₂ have been used for the detection of nicotinamide adenine dinucleotide and volatile organic compounds (Açikbaş et al., 2009; Galanin and Shaposhnikov, 2012; Pal et al., 2011). Physico-chemical properties of LuPc₂ complexes are utilized for the photoconversion of 4-nitrophenol (Zugle and Nyokong, 2012). Literature report reveals that incorporation of MPcs onto a silica support improves the efficacy of its catalytic performance (Armengol et al., 1999). Also MPcs grafted silica gel displayed antibactericidal activity (Kuznetsova et al., 2011). However MPcs incorporated onto silica matrix for electrocatalytic glucose biosensor application has been less studied. To further impart conductivity in bio-sensor construction, conducting polymers especially polyaniline (PANI) as electron transducers due to its excellent conductivity in its doped state, has been employed (Wang et al., 2014). Doping with poly(vinyl alcohol-vinyl acetate) itaconic acid (PVIA) may largely improve the processability, stability and cytocompatibility for biomedical application (Yin et al., 2017; Zeghioud et al., 2015). In this context, we intend to integrate the beneficial properties of silica, MPcs and PANI(PVIA) in the construction of a biosensor for effective GOx immobilization. Bearing in mind the challenges in the preparation of multicomponent based biosensing platforms, a new strategy has been employed for the integration of multicomponents (silica, LuPc₂ and PANI(PVIA)) into a conducting nanobead (CNB) formation. The objective is achieved through the preparation of water soluble LuPc₂; one-step incorporation of LuPc₂ into the porous SiO₂ nanocages (SiO₂(LuPc₂)) during its synthesis; instigating grafting approach for tagging (SiO₂(LuPc₂))

with PANI(PVIA) to obtain SiO₂(LuPc₂)-PANI(PVIA)-CNB. We also evaluated the GOx immobilized CNB as a high sensitive glucose biosensor.

Herein, we report on a facile preparation of SiO₂(LuPc₂)-PANI(PVIA)-CNB as electrochemical probe for the application of glucose biosensor. Nanoparticles of SiO₂(LuPc₂) were obtained by the Stöber method using TEOS and APTES as a precursor. PANI(PVIA) was obtained by oxidative polymerization of aniline followed by doping it with PVIA in THF. SiO₂(LuPc₂) nanoparticles were grafted with PANI(PVIA) through EDC/NHS chemistry to obtain SiO₂(LuPc₂)-PANI(PVIA)-CNB. The surface morphologies and other physico-chemical characteristics of SiO₂(LuPc₂)-PANI(PVIA)-CNB were investigated. An amperometric glucose biosensor was constructed by immobilization of GOx onto SiO₂(LuPc₂)-PANI(PVIA)-CNB coated screen printed carbon electrode.

2. Experimental

2.1. Chemicals

Tetraethyl orthosilicate (TEOS, 99.9%), 3-Aminopropyltriethoxysilane (APTES, 99%), ammonium hydroxide solution (NH₄OH) (28.0–30.0 wt% ammonia), Ethanol (≥99.9%), Poly(vinyl alcohol-vinyl acetate) itaconic acid (PVIA), aniline, *N*-(3-dimethylaminopropyl)-*N'*-ethylcarbodiimide hydrochloride (EDC hydrochloride), NHS (N-hydroxysuccinimide), ammonium persulfate (APS), D-(+)-glucose, glucose oxidase from aspergillus niger, Type X-S, lyophilized powder, 100,000-250,000 units/g solid (without added oxygen), glutaraldehyde solution (Grade II, 25% in H₂O), Potassium ferrocyanide, Potassium ferricyanide, potassium chloride (KCl), sodium chloride (NaCl), phosphate buffer saline (PBS, pH 7.0), ascorbic acid, uric acid, horse serum and human serum were all purchased from Sigma Aldrich (UK) and used as received. Polyethoxy substituted water soluble LuPc₂ was prepared following a previous method (Ayhan et al., 2013) but with a few modifications. To brief the double decker lutetium (III) compound was synthesised by the reaction of the dinitrile derivative with lutetium acetate in n-pentanol in the presence of DBU as a strong base.

2.2. Apparatus

The morphologies of the as prepared SiO₂(LuPc₂), PANI(PVIA) and SiO₂(LuPc₂)-PANI(PVIA)-CNB were examined by FEI-Nova scanning electron microscopy (SEM) with a low magnification (200,000×) and high voltage (20 kV). A Philips CM20 transmission electron microscopy (TEM) was used to obtain high resolution images operating at a voltage

of 200kV. UV–Visible spectrophotometer (Varian 50-scan UV–Visible) was used to measure the absorption spectra of the platform. FT-IR spectra of pristine and integrated CNB were recorded on a Perkin Elmer Spectrum 100 spectrophotometer. The Brunauer–Emmett–Teller (BET) surface area of the platform was investigated through nitrogen adsorption–desorption isotherm measurements and performed on a Micromeritics ASAP 2020 M volumetric adsorption analyzer at 77.34 K. A precision measurement to the platform surface was carried out by using a computer programmed Philips X-Pert X-ray diffractometer to be employed for the X-ray diffraction (XRD) work, using a Cu K α radiation source ($\lambda = 0.154056$ nm for K α 1) working at 40 KV and 40 mA. Electrochemical measurements were performed using a portable multi Potentiostat μ Stat 8000/8 channels purchased from DropSens (Spain) and controlled by PC with DropView 8400 software. Disposable screen-printed carbon electrodes (DRP-C110) from DropSens with 4 mm diameter working electrode (carbon) were used for modification. The auxiliary and reference electrodes are carbon and silver, respectively, while the tr ager (carrier) is ceramic. The basal carbon working electrodes were modified with pristine SiO₂(LuPc₂) or PANI(PVIA) or SiO₂(LuPc₂)-PANI(PVIA)-CNB for electrochemical purpose. The electroactivity of SiO₂(LuPc₂)-PANI(PVIA)-CNB modified electrode was evaluated by recording cyclic voltammogram (CV) in potassium ferro/ferricyanide solution containing 0.1 M NaCl in the potential range from -0.5 V to +0.5 V. Electrochemical impedance spectroscopy (EIS) measurements were carried out in the frequency range between 10 and 2000000 Hz. The amperometric responses of the fabricated SiO₂(LuPc₂)-PANI(PVIA)/GOx-CNB biosensor towards glucose detection were recorded under stirred conditions in 0.1 M PBS (pH 7.0) containing 0.1M NaCl by applying a constant potential of +0.2 V at the working electrode. The electrolyte solution was saturated with N₂ gas to remove dissolved oxygen prior to individual measurements. All electrochemical experiments were carried out at room temperature.

2.3. Preparation of SiO₂(LuPc₂)-PANI(PVIA)-CNB

The preparation of SiO₂(LuPc₂)-PANI(PVIA)-CNB involves two stages: (i) pristine synthesis of SiO₂(LuPc₂) nanoparticles and PANI(PVIA); (ii) formation of CNB. (ia) *Synthesis of SiO₂(LuPc₂)*: Monodispersed LuPc₂ incorporated SiO₂-NH₂ nanoparticles (SiO₂(LuPc₂)) was achieved through modified St ber method (Han et al., 2017). Briefly, water soluble LuPc₂ (10% V/V) was added to TEOS (3 mL) in NH₄OH/ethanol mixture (7:100 V/V). The mixture solution was allowed to stir for about 12 h followed by quick addition of 4 mL of APTES to the above mixture and continued stirring for another 12 h at room temperature. The resultant

colloidal LuPc₂ incorporated SiO₂-NH₂ (SiO₂(LuPc₂)) was obtained by centrifugation and washed with ethanol for three times; (ib) *Synthesis of PANI(PVIA)*: PANI(PVIA) was prepared by doping PANI-EB onto PVIA backbone. PANI-EB was prepared as reported in the literature (Nobrega et al., 2012). Doping was achieved by mixing 1 g of PANI-EB in a THF dispersion with appropriate quantity of PVIA (0.1 M) solution. The suspension was sonicated for about 2 h followed by electromagnetic stirring (6 h) at room temperature to make the dispersion homogeneous. The resultant PANI-PVIA dispersant was filtered through polycarbonate membrane (pore size: 0.2 mm) and washed several times with water till the filtrate became colorless. The precipitate was dried in vacuum oven at 60 °C for 24 h to obtain PANI(PVIA) powder. (ii) *Formation of CNB*: CNB structure of SiO₂(LuPc₂)-PANI(PVIA) was obtained through covalent grafting of COOH groups in PANI(PVIA) with NH₂ groups in SiO₂(LuPc₂) nanoparticles. About 0.05 g of dispersed PANI(PVIA) and 0.05 g of SiO₂(LuPc₂) were redispersed in 80 mL of 0.1M PBS solution (pH 7.0). 20 mL of EDC and NHS solutions (each 25 mM) were added and stirred for about 30 min. The dispersant solution was kept undisturbed at 25 °C for 24 h. The residue (SiO₂(LuPc₂)-PANI(PVIA)) was separated by centrifugation, washed with water and dried at room temperature.

2.4 Fabrication of SiO₂(LuPc₂)-PANI(PVIA)/GOx-CNB biosensor

About 10 mg of as prepared SiO₂(LuPc₂)-PANI(PVIA) was dispersed in 1 mL of isopropyl alcohol/naion mixture (7:3 V/V). 2 µl from the above stock solution was drop casted onto pre-cleaned screen-printed carbon electrode and dried at room temperature. SiO₂(LuPc₂)-PANI(PVIA)/GOx-CNB biosensor was fabricated by simultaneous drop casting GOx (1 µl) (10 mg in 1 mL PBS (pH 7.0)) and glutaraldehyde (1 µl) solution. The modified electrodes were dried at room temperature under N₂ atm for further analysis. Similarly, the other two SiO₂(LuPc₂)/GOx and PANI(PVIA)/GOx biosensors were fabricated.

3. Results and Discussion

3.1. Preparation of SiO₂(LuPc₂)-PANI(PVIA)/GOx-CNB

The various stages in the formation of SiO₂(LuPc₂)-PANI(PVIA)/GOx-CNB are presented as scheme 1; Stage 1 involves synthesis of SiO₂(LuPc₂) nanoparticles and PANI(PVIA); Stage 1a): SiO₂(LuPc₂) nanoparticles were obtained by synthesis of water soluble LuPc₂ as described in 2.3 and subsequent incorporation into SiO₂ nanoparticle through mixed hydrolysis/polycondensation of TEOS and APTES in NH₄OH/ethanol medium. The

incorporation of LuPc₂ was achieved through direct encapsulation into SiO₂ nanoparticles through Lu-O-Si bond formation during silanization process (Sorokin et al., 2001; B. Zhao et al., 2009). The colour of the SiO₂(LuPc₂) nanoparticles turns slightly yellow after 24 h of gelation time in contrast to misty white observed in pristine SiO₂ nanoparticle synthesis. This confirms the presence of LuPc₂ in the synthesized SiO₂(LuPc₂) nanoparticles. To further demonstrate the presence of LuPc₂ in the SiO₂ nanoparticles UV-visible spectra were recorded (discussed in section 3.2). Stage 1b): Synthesis of PANI(PVIA) was achieved by polymeric acid doping method (Taşdelen, 2017). The itaconic acid/acetate doping onto the PANI structure was confirmed by the slow colour change of PANI-EB from blue to green (Scheme 1, see: photograph of PANI(PVIA)). Doping was further confirmed by the change in the viscosity of the PANI-PVIA mixture solution. The –COOH/acetate groups of PVIA doped onto nitrogen atoms of PANI are connected to both benzene and quinone rings. It is to be noted that upon PVIA doping the solubility of PANI greatly enhanced (verified by dissolving PANI(PVIA) and PANI-EB in water). The PANI(PVIA) in water remains unsettled over a period of 48 hrs. Stage 2 involves formation of CNB structure from the above synthesized SiO₂(LuPc₂) nanoparticles and PANI(PVIA). The CNB formation was achieved through amide bond formation (amidation) via EDC/NHS chemistry (Booth et al., 2015; Qu et al., 2015). The excess –COOH group in PANI(PVIA) was covalently linked to –NH₂ sites in SiO₂(LuPc₂) by carbodiimide activation with the assistance of NHS, leading to conjugation (Olde Damink et al., 1996; Pattabiraman and Bode, 2011). In this work, we have chosen SiO₂, LuPc₂, PANI, PVIA for CNB formation due to the following reasons. The simultaneous incorporation of LuPc₂ during SiO₂ synthesis leads to the formation of porous cage over LuPc₂ particles. The SiO₂ cage formation over LuPc₂ protects it from leaching and maintains the functionalities at diverse environment. The SiO₂ cage was made conductive by grafting it with PANI(PVIA). The multiple functional groups in PVIA assist grafting PANI onto SiO₂(LuPc₂) nanoparticle. Furthermore PVIA also offers biocompatibility/stability of CNB at different pH (Mishra et al., 2011). Thus, SiO₂(LuPc₂)-PANI(PVIA)-CNB can have the beneficial characteristics of an electron conductive PANI backbone, the electron mediating property of LuPc₂, while SiO₂ to protect leaching of catalyst and PVIA to offer biocompatibility to the CNB structures. The final product was greenish white resulted from the covalent grafting of PANI(PVIA) onto the surface of SiO₂(LuPc₂) nanoparticles.

3.2. Morphology

SiO₂(LuPc₂) nanoparticles exhibited similar spherical morphology (Fig. 1(a)) as that of pristine SiO₂ nanoparticles (Fig. 1(d)), except with the change in the size of the nanoparticles. Fig. 1(a) shows spherical particles of SiO₂(LuPc₂) in different size distribution. The particle size ranges from 150 to 200 nm. However, the as prepared pristine SiO₂ nanoparticles are uniform with an average size of 140 nm (Fig. 1(d)). The variation in the size distribution of SiO₂(LuPc₂) exemplifies the incorporation of LuPc₂ into SiO₂ nanoparticles during the mode of synthesis. Furthermore it could be seen that the particles are slightly tilted to accommodate LuPc₂ in its interior porous structure. The presence of LuPc₂ in SiO₂(LuPc₂) nanoparticles was further confirmed through EDX measurements. The elemental test results confirmed the presence of inorganic ion Lu (24.2 wt%) in the ratio of 1:3 with SiO₂ (Fig.1(b)) within SiO₂(LuPc₂) nanoparticles. Fig. 1(c) shows the morphology of SiO₂(LuPc₂)-PANI(PVIA)-CNB. Upon PANI(PVIA) grafting onto SiO₂(LuPc₂), the size of the nanoparticles transformed between 180 to 220 nm. This ensures the successive grafting of PANI(PVIA) onto the surface of SiO₂(LuPc₂) nanoparticles (Roosz et al., 2017). For further confirmation TEM image of SiO₂(LuPc₂)-PANI(PVIA)-CNB is recorded (Fig. 1g). The dark spots noticed within the SiO₂ nanoparticles ensure the incorporation of LuPc₂ inside the nanocages of SiO₂. However, the TEM image of pristine SiO₂ nanoparticle showed smooth and uniform size distribution of particles (Fig. 1h). On closer analysis, we could notice that the surface becomes coarse due to PANI(PVIA) grafting. For reference the SEM images of PANI(PVIA) and LuPc₂ are shown in Fig. 1(e) and Fig. 1(f), respectively. TEM image of PANI(PVIA) exhibited nanobead like structure with average particle size around 30 nm (Fig. 1i).

The surface area of pristine SiO₂ and SiO₂(LuPc₂) are studied through Brunauer, Emmett and Teller (BET) measurements. The surface area of pristine SiO₂ and SiO₂(LuPc₂) are found to be 48.2889 ± 0.8737 m²/g and 20.4619 ± 0.5225 m²/g respectively. The reduction in the surface area ~57% addresses the incorporation of LuPc₂ well within porous nanocage of SiO₂ nanoparticles. The results are analogous to the significant decrease in the specific surface area noticed in palladium immobilized nanocages of SBA-16 compared to parent SBA-16 (Wang et al., 2013).

3.3. UV-visible spectroscopy

The UV-visible absorption spectra of SiO₂(LuPc₂) (Fig. 2a) show characteristic N, B, and Q bands of LuPc₂ around $\lambda = 315$ nm, sharp band around $\lambda = 390$ nm, and intensive Q absorption band of the macrocycles at $\lambda = 702$ nm (Basova et al., 2008a; 2008b). This

features the incorporation of LuPc₂ inside SiO₂ nanoparticles. However the observed variation in peak intensity in addition to small shift in absorption bands compared to pristine LuPc₂ (Fig. 2,inset) may arise due to the interaction of LuPc₂ with host walls of SiO₂ and dimerization of larger aggregates during the gelation process (Holland et al., 1998). Fig. 2 b,c shows the absorption spectra of PANI-EB and PANI(PVIA), respectively. The undoped PANI-EB (Fig. 2b) showed absorption bands corresponding to π - π^* transition of benzene ring (310 nm) and excitation of the imine segment on the PANI chain (around 600 nm) (Rahy et al., 2011). Moreover for PANI(PVIA) (Fig. 2c), the disappearance of the band around 600 nm indicates that the doping occurs at the imine segment of the emeraldine chain (Wang et al., 2014). The observed bathochromic (red) shift of π -polaron to > 750 nm illustrates that PANI backbone was well doped with -COOH/acetate functional groups in PVIA (Taşdelen, 2017). Additionally, the appearance of the band at 420 nm results from the polaron phenomenon of PANI(PVIA) (Dominis et al., 2002). In the case of SiO₂(LuPc₂)-PANI(PVIA), the polaronic band of PANI(PVIA) exhibits hypsochromic shift to around 360 nm (Fig. 2d) with broadening of the Q band around 700 nm. This ensures that PANI(PVIA) grafting over SiO₂(LuPc₂) (~30 nm thickness calculated from SEM) does insignificantly affect the electronic properties of LuPc₂ (Zhuang et al., 2011). The other physicochemical characteristics such as FTIR and XRD patterns of pristine SiO₂(LuPc₂) and CNB are presented in the Supporting Information (SI) SI-1.

3.4. Electrochemical impedance measurements

Electrochemical impedance spectroscopy is a powerful tool to study interfacial characteristics of surface modified electrodes as well as gaining information about charge transfer properties of the various compounds incorporated in the electrode to support the function of the modifiers. SI-2(A) shows the impedance measurements (Nyquist plot) of SiO₂(LuPc₂), PANI(PVIA) and SiO₂(LuPc₂)-PANI(PVIA) respectively carried out at the open circuit potential in 5 mM K₃[Fe(CN)₆]/K₄[Fe(CN)₆] containing 0.1 M NaCl. One could observe distinct differences in the impedance spectra. The charge transfer resistance (R_{ct}) was calculated from the obtained semicircular part at the high frequency region. The results showed that SiO₂(LuPc₂)-PANI(PVIA)-CNB exhibits much lower R_{ct} value (180 Ω) compared to SiO₂(LuPc₂) (1380 Ω) and PANI(PVIA) (1710 Ω) modified electrodes. The electron transfer rate at SiO₂(LuPc₂)-PANI(PVIA)-CNB biosensor was approximately 7.6 and 9.5 higher than that at SiO₂(LuPc₂) and PANI(PVIA) electrodes, respectively. The reduction in the resistance to charge transfer in the electrode is possibly accomplished by the

LuPc₂, as clearly indicated in SI-2(A) curve (d). The linear part at low frequency region ensures a mixed kinetic and diffusion controlled process at SiO₂(LuPc₂)-PANI(PVIA)-CNB biosensor while surface controlled process prevails at pristine SiO₂(LuPc₂) and PANI(PVIA) modified electrodes (based on tail length). The fast electron transfer rate at SiO₂(LuPc₂)-PANI(PVIA)-CNB informs that the grafted PANI(PVIA) chains electronically wires the electron from the surface through LuPc₂ to the underlying electrode. For comparison the Nyquist plot of LuPc₂ and SiO₂ is also presented. Equivalent circuit model R(Q(R(QR))) for the fabricated biosensor, SiO₂(LuPc₂)-PANI(PVIA)-CNB, where R_s is the uncompensated solution resistance; R_{et} is the electron transfer resistance; R_w is Warburg diffusion element (W) and CPE₁ & CPE₂ standing for the double layer capacitance on the electrode/electrolyte interface and the pseudocapacitance in the polymer film, respectively, is shown in SI-2(B).

3.5. Electrochemical behavior of SiO₂(LuPc₂)-PANI(PVIA)-CNB modified electrode

The electrochemical behavior of the modified electrodes was investigated by recording cyclic voltammograms (CVs) of modified electrodes using Fe(CN)₆^{3-/4-} as a redox marker. CV obtained at pristine SiO₂ (curve a), SiO₂(LuPc₂) (curve b), PANI(PVIA) (curve c) and SiO₂(LuPc₂)-PANI(PVIA)-CNB (curve d) in Fe(CN)₆^{3-/4-} (5 mM) containing 0.1M NaCl is shown in Fig. 3(A). A pair of one electron quasi-reversible redox peaks corresponding to Fe(II)/Fe(III) transition process was observed at all electrodes. However, the redox peak current (I_{pa}/I_{pc}) and the peak potential separation between anodic (E_{pa}) and cathodic (E_{pc}) wave (ΔE_p) differ between the individual electrodes. It is observed that the I_{pa}/I_{pc} value of SiO₂(LuPc₂) increases by ~1.2 times than that of pristine SiO₂ modified electrode. This ensures that the incorporated LuPc₂ within SiO₂ cage enhances the electrochemical activity of SiO₂ (García-Sánchez et al., 2013). Moreover the I_{pa}/I_{pc} redox peak current further increases to 181.4 μA /-168.4 μA (I_{pa}/I_{pc}) at SiO₂(LuPc₂)-PANI(PVIA)-CNB modified electrode (curve d). It should be noted that the Fe(II)/Fe(III) redox peak current is found to be highest at SiO₂(LuPc₂)-PANI(PVIA)-CNB which is ~1.3 and ~1.5 times higher than at SiO₂(LuPc₂) and pristine SiO₂ nanoparticles modified electrodes. The result demonstrates that the presence of PANI(PVIA) as a grafted network onto SiO₂(LuPc₂) augments the electronic conductivity (Gopalan et al., 2010), in addition to the presence of LuPc₂ and SiO₂ that provide three dimensional pathway for the adequate percolation of ions to the electrode surface and facilitate the electron transfer process (Al-Sagur et al., 2017; Gopalan et al., 2009). The I_{pa}/I_{pc} redox peaks of pristine PANI(PVIA) are ~5.1 times lower than that in the case of SiO₂(LuPc₂)-PANI(PVIA)-CNB modified electrode. The ΔE_p value was found to increase in

the following order: PANI (PVIA) (145 mV) < SiO₂(LuPc₂)-PANI(PVIA)-CNB (170 mV) < SiO₂(LuPc₂) (172 mV) < SiO₂ (175 mV).

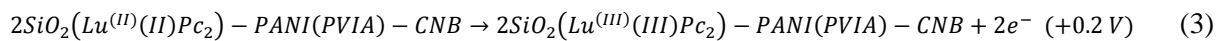
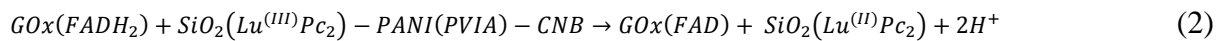
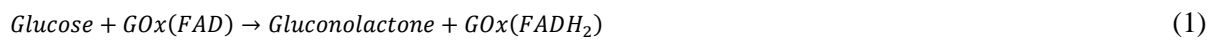
CVs of SiO₂(LuPc₂)-PANI(PVIA)-CNB were also recorded for different scan rates (10–100 mV/s) (SI-3). The calibration of $v^{1/2}$ vs I_{pa} or I_{pc} showed linearity with the correlation coefficient of 0.999 (n=10), which confers the diffusion controlled process of Fe(CN)₆^{3-/4-} redox reaction at SiO₂(LuPc₂)-PANI(PVIA)-CNB (Siswana et al., 2006). The diffusional coefficient (D) was calculated to be 8.106x10⁻⁶ cm²/s using Randles–Sevcik equation (Nagarale et al., 2009). With the known value of D and n=1 for reversible redox process, the electrochemical active surface area (A) of the electrode was determined to be 1.184 cm². The value of ‘A’ results from the three dimensional porous structures of SiO₂(LuPc₂)-PANI(PVIA)-CNB. The results from electrochemical activity (CV) demonstrate the importance of individual components (SiO₂, LuPc₂, PANI(PVIA)) in its fabrication design for the further immobilization of GOx for the determination of glucose.

3.6. Electrochemical behavior of SiO₂(LuPc₂)-PANI(PVIA)/GOx-CNB biosensor

CV response of the GOx immobilized SiO₂(LuPc₂)-PANI(PVIA)-CNB modified electrode in N₂-saturated PBS solution (pH 7.0) containing 0.1M NaCl is shown in Fig. 3B. A well-defined symmetrical redox peaks (0.074 V anodic; -0.212 V cathodic) corresponding to immobilized GOx at scan rate = 100 mV/s could be noticed. The effect of scan rate on the CV response of redox peaks was also studied by varying the scan rate from 100-500 mV/s. It should be noted that even at the higher scan rate of 500 mV/s, the SiO₂(LuPc₂)-PANI(PVIA)/GOx-CNB biosensor showed redox behavior with a slight shift in its ΔE_p. This ensures the stable immobilization of GOx onto SiO₂(LuPc₂)-PANI(PVIA)-CNB in its native configuration (Gopalan et al., 2009). The redox peak current linearly increased with $v^{1/2}$ in the range of 100–500 mV s (R² ≈ 0.999), indicating a diffusion-controlled electrochemical process. The plot of log $v^{1/2}$ vs E_{pa} and E_{pc} (inset Fig 3B) showed straight lines with the correlation coefficient of R² = 0.994 (anodic) and R² = 0.997 (cathodic). The diffusion coefficient (D) of charge transfer was estimated to be 1.47x10⁻⁶ cm²/s using Randles–Sevcik equation (Nagarale et al., 2009). The surface coverage of the modified electrode is calculated to be 7.13x10⁻⁷ mol/cm² which is typically higher than GOx immobilized on SAM modified electrode (4.80x10⁻¹² mol/cm²) (Fang et al., 2003). The higher value of surface coverage admits the increased loading of GOx onto SiO₂(LuPc₂)-PANI(PVIA)-CNB surface. Moreover the immobilized GOx enzymes are well bound on the surface observed from the redox peaks

at scan rate = 500 mV/s in 0.1 M PBS. Thus the higher and native loading of GOx could be achieved by the excess functional groups (from PVIA&PANI) and biocompatible environment provided by PVIA for the guest enzymes. For comparison CVs of pristine SiO₂(LuPc₂)/GOx and PANI(PVIA)/GOx were also recorded in 0.1M PBS and presented in SI-4.

3.7. Amperometric response of glucose at SiO₂(LuPc₂)-PANI(PVIA)/GOx-CNB biosensor
Amperometric measurements were recorded for varied concentrations of glucose to demonstrate the functioning of SiO₂(LuPc₂)-PANI(PVIA)/GOx-CNB as a potential glucose biosensor and the results are shown in Fig. 4. Optimization of experimental parameters for recording amperometric measurements were presented in SI-5(i-iii). Upon successive injection of glucose (1 mM) at regular intervals, a rapid and prominent increase in the bioelectrocatalytic amperometric current (E = +0.2 V) was observed under stirred condition. The operating principle is based on the enzymatic oxidation of glucose catalyzed by GOx immobilized onto SiO₂(LuPc₂)-PANI(PVIA)-CNB. The injected glucose are first enzymatically oxidized to gluconolactone, while GOx(FAD) reduced to GOx(FADH₂). Thereafter GOx(Red) will be regenerated to GOx(FAD) by electrooxidized SiO₂(LuPc₂)-PANI(PVIA)-CNB. The plausible mechanism is as follows



The current response was linear for glucose concentration in the range of 1–16 mM (correlation coefficient, $R = 0.997$) (Fig. 4 inset). The responses were saturated when glucose concentrations were higher than 16 mM that could be attributed to enzyme saturation (Li et al., 2009). The sensitivity of the SiO₂(LuPc₂)-PANI(PVIA)/GOx-CNB biosensor is calculated to be 38.53 $\mu\text{A}/\text{mM}/\text{cm}^2$ from the slope of the calibration plot with a RSD of 5.8%. The sensitivity of the SiO₂(LuPc₂)-PANI(PVIA)/GOx-CNB biosensor is superior than reported for the glucose biosensor fabricated with other SiO₂ composites for GOx immobilization. Sol-gel/GOx/copolymer (0.6 $\mu\text{A}/\text{mM}$) (Wang et al., 1998), PEDOT/PB/MWNT (2.67 $\mu\text{A}/\text{mM}$) (Chiu et al., 2009), Silica/GOx/CNTs (approximately 0.2 $\mu\text{A}/\text{mM}$) (Salimi et al., 2004), and GOx-SWCNT conjugates/PVI-Os bilayers (32 $\mu\text{A}/\text{mM}/\text{cm}^2$) (Gao et al., 2011) are typical examples as reported in the literature. The

superior sensitivity results from the judicious design of the fabricated electrode. The presence of thin grafted PANI(PVIA) layer provides excess functional groups (-OH/ -CH₃COO-/ -COOH from PVIA and NH₂ sites from PANI) for the bonding of GOx. Also PVIA provides biocompatible environment for the immobilized (GOx) enzyme (biocompatibility of poly itaconic acid for biomolecules). While SiO₂ provides three dimensional porous surface for the grafting process, LuPc₂ in SiO₂ nanoparticles mediates/transfers electrons to the electrode surface. The SiO₂(LuPc₂)-PANI(PVIA)/GOx-CNB biosensor showed a fast response to the changes in glucose concentration and the steady-state response current reached within 2 s. The response time is much lower than in the case of pristine PANI incorporated silica particles (Manesh et al., 2010), SiO₂ grafted with PVA+PVP (Wang et al., 1998), and mesacellular carbon foam (Wang et al., 1998). The instant amperometric current response upon the addition of glucose is attributed to the faster diffusion of glucose at SiO₂(LuPc₂)-PANI(PVIA)/GOx-CNB. The rapid response to glucose was achieved due to the integrated presence of PANI(PVIA) that electronically wires the electron from GOx through LuPc₂ to underlying electrode (Tiwari et al., 2015). The wide linear range (1-16 mM) and high sensitivity (38.53 $\mu\text{A}/\text{mM}/\text{cm}^2$) of SiO₂(LuPc₂)- PANI(PVIA)/GOx-CNB biosensor made it suitable for human blood glucose detection.

The apparent Michaelis–Menten constant (K_M) was calculated as 10.36 mM using the slope and intercept values from the Lineweaver–Burk plot for SiO₂(LuPc₂)- PANI(PVIA)/GOx-CNB biosensor (Mobin et al., 2010). The value is close to that reported for the free GOx enzyme (12.4 mM) (Swoboda and Massey, 1965). This demonstrates that non-denaturated characteristics of GOx immobilized onto SiO₂(LuPc₂)- PANI(PVIA)-CNB. The limit of detection (LOD) for glucose at PAA-rGO/Vs-PANI/LuPc₂/GOx-MFH biosensor was calculated as 0.1 mM (signal to noise ratio=3). The detection limit is estimated as three times of the standard deviation of the background. Comparison of analytical performances of some glucose biosensors based on GOx immobilized onto PANI/phthalocyanine/silica as one of the component in the matrix is presented in SI-6, Table 1.

3.8. Repeatability, Reproducibility and stability of SiO₂(LuPc₂)- PANI(PVIA)/GOx biosensor

To investigate the stability of the SiO₂(LuPc₂)- PANI(PVIA)/GOx biosensor, (preserved in 0.1M PBS at 4 °C), amperometric current response was recorded at regular intervals for a period of 45 days (SI-7(i)). After two week time the SiO₂(LuPc₂)- PANI(PVIA)/GOx biosensor retained 98.7% of its initial current response (glucose 4mM). By the end of 45 days, 96.4% of the initial current response was restored. These results confirmed that the

functioning of GOx immobilized onto SiO₂(LuPc₂)- PANI(PVIA)-CNB was well protected because of the co-presence of PVIA and SiO₂ nanoparticles in the fabricated biosensor (Işiklan et al., 2009). The leaching effect of immobilized GOx from the fabricated SiO₂(LuPc₂)-PANI(PVIA)-CNB/GOx biosensor was investigated by recording cyclic voltammetry after immersion of the test electrode in 0.1M PBS for a period of 1h. From the characteristic redox peaks of GOx, it is confirmed that there is insignificant leaching of GOx from the fabricated biosensor. Also the leaching effect of LuPc₂ in the pristine SiO₂(LuPc₂) electrode was also tested after immersion in Fe(CN)₆^{3-/4-} (5 mM) for the time period of 30 min. It was observed from CV (recorded at the scan rate of 50 mV/s) that the redox peak current does not vary before and after immersion. This confirms that LuPc₂ is well incorporated within the host SiO₂ porous cage and hence protected from leaching to the background solution that is usually observed in many mediator based biosensor electrodes (Wang et al., 2015).

To examine the reproducibility of SiO₂(LuPc₂)-PANI(PVIA)-CNB/GOx biosensor, seven electrodes were prepared under identical conditions and stored at 4°C. Amperometric current response was recorded in optimized conditions for three different concentrations of glucose (low, normal and high) (SI-7(ii)). The relative standard deviations (RSD) for glucose were 2.8 % (2mM), 1.3% (4mM) and 4.9% (9 mM). The relatively low RSD value indicated that SiO₂(LuPc₂)-PANI(PVIA)-CNB/GOx biosensor exhibited good reproducibility in all levels of glucose. The repeatability of SiO₂(LuPc₂)-PANI(PVIA)-CNB/GOx biosensor for 5 consecutive measurements of glucose (4 mM) was estimated to RSD = 1.4% under ideal conditions (SI-7(iii)).

3.9. Specificity and interference

The selectivity of the fabricated electrode is an important criterion for biosensor application. Under the applied potential of +0.2 V, the presence of interfering substances hardly affects the amperometric current response of glucose at SiO₂(LuPc₂)-PANI(PVIA)-CNB/GOx biosensor. Repetitive measurements of glucose (4 mM) in the presence of interfering substances such as dopamine (DA), lactic acid (LA), ascorbic acid (AA) and uric acid (UA) (2 mM each), are shown in SI-8. DA and UA at the concentration of 2 mM produced the relative low response of ~ 2.2% and ~ 5.0%, indicating that these species coexisting in the sample matrix did not affect the determination of glucose. This informs that SiO₂(LuPc₂)-PANI(PVIA)-CNB/GOx biosensor exhibits relatively selective detection of glucose and can

be potentially applied for serum samples even in the presence of higher concentration of electrochemically active substances.

3.10. Glucose determination in real samples at SiO₂(LuPc₂)-PANI(PVIA)/GOx-CNB biosensor

The suitability of SiO₂(LuPc₂)-PANI(PVIA)/GOx-CNB biosensor in the determination of glucose in real samples was examined. A continuous amperometry was recorded as shown in SI-9(i) at optimized conditions (E= +0.2V) in the presence of diluted (using 0.1M PBS to obtain required concentration) fruit juices and horse serum sample. The results obtained for a typical determination of glucose by standard additions method are presented in SI-9(i) Table 2. The results in SI-9 Table 2, indicate that the percentage recovery ranged from 89.72 to 105 %, which agrees with other standard spectrophotometric method. The satisfactory results demonstrate the practical usage of the fabricated biosensor. Direct determination of glucose in human and horse serum samples at SiO₂(LuPc₂)-PANI(PVIA)/GOx-CNB biosensor was also carried out at optimized condition (SI-9(ii)). From the amperometric response, it could be understood that the fabricated SiO₂(LuPc₂)-PANI(PVIA)/GOx-CNB biosensor responded well for real samples.

4. Conclusions

In this work, we have successfully prepared a multicomponent based conducting nanobead (CNB) comprising lutetium phthalocyanine (LuPc₂), SiO₂ nanoparticle, polyaniline (PANI) and poly (vinyl alcohol-vinyl acetate-itaconic acid) (PVIA). The prepared CNB was utilized as the platform for the immobilization of glucose oxidase (GOx). The new fabricated SiO₂(LuPc₂)-PANI(PVIA)/GOx-CNB biosensor has shown good sensitivity (38.53 $\mu\text{A.mM}^{-1}\text{cm}^{-2}$) with wide linear range (1-16 mM) for the amperometric detection of glucose. The SiO₂(LuPc₂)-PANI(PVIA)/GOx-CNB biosensor has exhibited a specific and fast response (~2s) on addition of glucose. The proposed SiO₂(LuPc₂)-PANI(PVIA)/GOx-CNB biosensor showed good accuracy for both juice and serum samples, providing the potential feasibility for its use in Industrial&Clinical analysis. In addition to its use as a glucose sensor, the CNB can be utilized as a platform for the construction of other biosensors in future.

Acknowledgements

Hadi Al-Sagur acknowledges the financial support provided for his PhD study from the Ministry of Higher Education and Scientific Research (MOHESR) and the College of Medicine/Thi Qar University in the south of Iraq. H. Karakaş, D. Atilla, A. G. Gürek acknowledge the research fund by Gebze Technical University (Project No.: 2017-A-101-01). T. Basova acknowledges the research fund by Nikolaev Institute of Inorganic Chemistry, Russia (basic project).

References

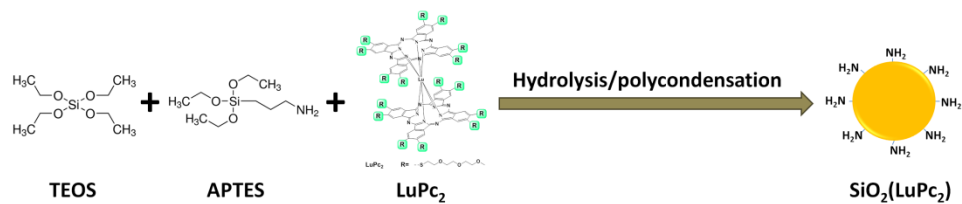
- Açıkbaş, Y., Evyapan, M., Ceyhan, T., Çapan, R., Bekaroğlu, Ö., 2009. *Sensors Actuators, B Chem.* 135, 426–429.
- Al-Sagur, H., Komathi, S., Khan, M.A., Gurek, A.G., Hassan, A., 2017. *Biosens. Bioelectron.* 92, 638–645.
- Armengol, E., Corma, A., Forne, V., Garcõ, H., Primo, J., 1999. *Appl. Catal. A Gen.* 181, 305–312.
- Ayhan, M.M., Altınbaş Özpinar, G., Durmuş, M., Gürek, A.G., 2013. *Dalt. Trans.* 42, 14892.
- Basova, T., Jushina, I., Gürek, A.G., Ahsen, V., Ray, A.K., 2008. *J. R. Soc. Interface* 5, 801–6.
- Basova, T., Plyashkevich, V., Hassan, A., 2008. *Surf. Sci.* 602, 2368–2372.
- Binnemans, K., 2005. Rare-earth beta-diketonates. *Handb. Phys. Chem. Rare Earths* 35, 107–272.
- Booth, M.A., Kannappan, K., Hosseini, A., Partridge, A., 2015. *Langmuir* 31, 8033–8041.
- Brian T. Holland, Chad Walkup, A., Stein*, A., 1998. *J. Phys. Chem. B* 102, 4301–4309.
- Chiu, J.Y., Yu, C.M., Yen, M.J., Chen, L.C., 2009. *Biosens. Bioelectron.* 24, 2015–2020.
- Cui, L., Lv, G., He, X., 2015. *J. Power Sources* 282, 9–18.
- Dominis, A.J., Spinks, G.M., Kane-Maguire, L.A.P., Wallace, G.G., 2002. *Synth. Met.* 129, 165–172.
- Fang, A., Ng, H.T., Li, S.F.Y., 2003. *Biosens. Bioelectron.* 19, 43–49.
- Fang, Y.-S., Huang, X.-J., Wang, L.-S., Wang, J.-F., 2015. *Biosens. Bioelectron.* 64, 324–32.
- Galanin, N.E., Shaposhnikov, G.P., 2012. *J. Gen. Chem.* 82, 1734–1739.
- Galant, A.L., Kaufman, R.C., Wilson, J.D., 2015. *Food Chem.* 188, 149–160.

- 1 Gao, Q., Guo, Y., Zhang, W., Qi, H., Zhang, C., 2011. *Sensors Actuators, B Chem.* 153, 219–
2 225.
- 3 García-Sánchez, M.A., Rojas-González, F., Menchaca-Campos, E.C., Tello-Solís, S.R.,
4 Quiroz-Segoviano, R.I.Y., Diaz-Alejo, L.A., Salas-Bañales, E., Campero, A., 2013.
5 *Molecules* 18, 588–653.
- 6 Gopalan, A.I., Lee, K.P., Komathi, S., 2010. *Biosens. Bioelectron.* 26, 1638–1643.
- 7 Gopalan, A.I., Lee, K.P., Ragupathy, D., Lee, S.H., Lee, J.W., 2009. *Biomaterials* 30, 5999–
8 6005.
- 9 Han, Y., Lu, Z., Teng, Z., Liang, J., Guo, Z., Wang, D., Han, M.Y., Yang, W., 2017.
10 *Langmuir* 33, 5879–5890.
- 11 He, Q., Zhang, J., Shi, J., Zhu, Z., Zhang, L., Bu, W., Guo, L., Chen, Y., 2010. *Biomaterials*
12 31, 1085–1092.
- 13 International Diabetes Federation, 2006. *Diabetes Atlas - third edition*, Journal of Chemical
14 Information and Modeling.
- 15 Işiklan, N., Kurşun, F., Inal, M., 2009. *J. Appl. Polym. Sci.* 114, 40–48.
- 16 Jaganathan, H., Godin, B., 2012. *Adv. Drug Deliv. Rev.* 64, 1800–1819.
- 17 Kuznetsova, N. a., Yuzhakova, O. a., Strakhovskaya, M.G., Shumarina, A.O., Kozlov, A.S.,
18 Krasnovsky, A. a., Kaliya, O.L., 2011. *J. Porphyr. Phthalocyanines* 15, 718–726.
- 19 Li, J., Wei, X., Yuan, Y., 2009. *Sensors Actuators, B Chem.* 139, 400–406.
- 20 Li, Q., Luo, G., Wang, Y., Zhang, X., 2000. *Mater. Sci. Eng. C* 11, 67–70.
- 21 Manesh, K.M., Santhosh, P., Uthayakumar, S., Gopalan, A.I., Lee, K.P., 2010. *Biosens.*
22 *Bioelectron.* 25, 1579–1586.
- 23 Mani, V., Devasenathipathy, R., Chen, S.M., Huang, S.T., Vasantha, V.S., 2014. *Enzyme*
24 *Microb. Technol.* 66, 60–66.
- 25 Mishra, R.K., Majeed, A.B.A., Banthia, A.K., 2011. *Int. J. Plast. Technol.* 15, 21–32.
- 26 Mobin, S.M., Sanghavi, B.J., Srivastava, A.K., Mathur, P., Lahiri, G.K., 2010. *Anal. Chem.*
27 82, 5983–5992.
- 28 Nagarale, R.K., Lee, J.M., Shin, W., 2009. *Electrochim. Acta* 54, 6508–6514.
- 29 Nobrega, M.M., Silva, C.H.B., Constantino, V.R.L., Temperini, M.L.A., 2012. *J. Phys. Chem.*
30 *B* 116, 14191–14200.
- 31 Olde Damink, L.H.H., Dijkstra, P.J., Van Luyn, M.J.A., Van Wachem, P.B., Nieuwenhuis, P.,
32 Feijen, J., 1996. *Biomaterials* 17, 765–773.
- 33 Olgac, R., Soganci, T., Baygu, Y., Gök, Y., Ak, M., 2017. *Biosens. Bioelectron.* 98, 202–209.
- 34 Pal, C., Cammidge, a N., Cook, M.J., Sosa-Sanchez, J.L., Sharma, a K., Ray, a K., 2011. *J.*
35 *R. Soc. Interface* 74, 2848–2850.

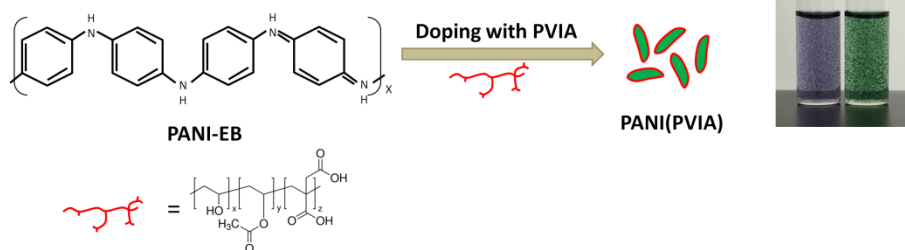
- 1 Pattabiraman, V.R., Bode, J.W., 2011. *Nature* 480, 471–9.
- 2 Peters, A.L., Buschur, E.O., Buse, J.B., Cohan, P., Diner, J.C., Hirsch, I.B., 2015. *Diabetes*
3 *Care* 38, 1687–1693.
- 4 Piao, Y., Han, D.J., Azad, M.R., Park, M., Seo, T.S., 2015. *Biosens. Bioelectron.* 65, 220–
5 225.
- 6 Qu, Z., Xu, H., Gu, H., 2015. *ACS Appl. Mater. Interfaces* 7, 14537–14551.
- 7 Rahy, A., Rguig, T., Cho, S.J., Bunker, C.E., Yang, D.J., 2011. *Synth. Met.* 161, 280–284.
- 8 Roosz, N., Euvard, M., Lakard, B., Buron, C.C., Martin, N., Viau, L., 2017. *J. Colloid*
9 *Interface Sci.* 502, 184–192.
- 10 Salimi, A., Compton, R.G., Hallaj, R., 2004. *Anal. Biochem.* 333, 49–56.
- 11 Shafiee, G., Mohajeri-Tehrani, M., Pajouhi, M., Larijani, B., 2012. *J. Diabetes Metab. Disord.*
12 11, 17.
- 13 Singh, M., Kathuroju, P.K., Jampana, N., 2009. *Sensors Actuators, B Chem.* 143, 430–443.
- 14 Siswana, M.P., Ozoemena, K.I., Nyokong, T., 2006. *Electrochim. Acta* 52, 114–122.
- 15 Sorokin, A.B., Buisson, P., Pierre, A.C., 2001. *Microporous Mesoporous Mater.* 46, 87–98.
- 16 Swoboda, B.E.P., Massey, V., 1965. *J. Biol. Chem.* 240, 2209–2215.
- 17 Tabish, S.A., 2007. *Int. J. Health Sci.* 1, V–VIII.
- 18 Taşdelen, B., 2017. *Polym. Adv. Technol.*
- 19 Tirimacco, R., Tideman, P.A., Dunbar, J., Simpson, P.A., Philpot, B., Laatikainen, T., Janus,
20 E., 2010. *Int. J. Diabetes Mellit.* 2, 24–27.
- 21 Tiwari, A., Patra, H.K., Turner, A.P., 2015. *John Wiley Sons* 373.
- 22 Wang, B., Li, B., Deng, Q., Dong, S., 1998. *Anal. Chem.* 70, 3170–3174.
- 23 Wang, H., Bu, Y., Dai, W., Li, K., Wang, H., Zuo, X., 2015. *Sensors Actuators, B Chem.* 216,
24 298–306.
- 25 Wang, H.B., Zhang, Y.H., Yang, H.L., Ma, Z.Y., Zhang, F.W., Sun, J., Ma, J.T., 2013. 168,
26 65–72.
- 27 Wang, Y., Zheng, H., Jia, L., Li, H., Li, T., Chen, K., Gu, Y., 2014. *J. Macromol. Sci. Part A*
28 51, 577–581.
- 29 Yin, Y., Dang, Q., Liu, C., Yan, J., Cha, D., Yu, Z., Cao, Y., Wang, Y., Fan, B., 2017. *Int. J.*
30 *Biol. Macromol.* 102, 10–18.
- 31 Zebda, A., Gondran, C., Le Goff, A., Holzinger, M., Cinquin, P., Cosnier, S., 2011. *Nat.*
32 *Commun.* 2, 370.
- 33 Zeghioud, H., Lamouri, S., Safidine, Z., Belbachir, M., 2015. *J. Serb. Chem. Soc* 8033513,
34 917–931.

- 1 Zhao, B., Yin, J.J., Bilski, P.J., Chignell, C.F., Roberts, J.E., He, Y.Y., 2009. Toxicol. Appl.
2 Pharmacol. 241, 163–172.
- 3 Zhao, Y., Trewyn, B.G., Slowing, I.I., Lin, V.S., 2009. Synthesis (Stuttg). 1–9.
- 4 Zhu, C., Yang, G., Li, H., Du, D., Lin, Y., 2014. Am. Chem. Soc. 1, 230–249.
- 5 Zhuang, Q.F., Wang, J.E., Zhu, Z.J., Li, F., Wang, Z.X., 2011. Fenxi Huaxue/ Chinese J.
6 Anal. Chem. 39, 1567–1571.
- 7 Zugle, R., Nyokong, T., 2012. J. Mol. Catal. A Chem. 358, 49–57.
- 8
- 9

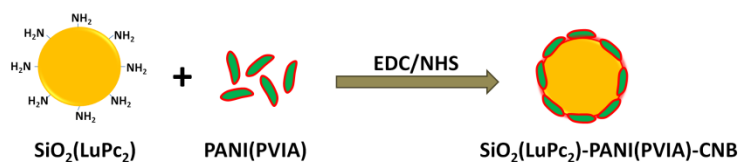
Stage 1: (i) Synthesis of $\text{SiO}_2(\text{LuPc}_2)$ nanoparticles



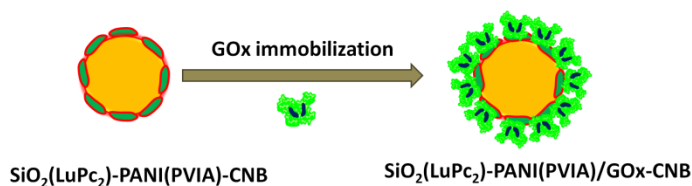
Stage 1: (ii) Synthesis of PANI(PVIA)



Stage 2: Preparation of $\text{SiO}_2(\text{LuPc}_2)$ -PANI(PVIA)-CNB



Fabrication of $\text{SiO}_2(\text{LuPc}_2)$ -PANI(PVIA)/GOx-CNB



Scheme 1 Schematic representation of the formation of $\text{SiO}_2(\text{LuPc}_2)$ -PANI(PVIA)/GOx-CNB

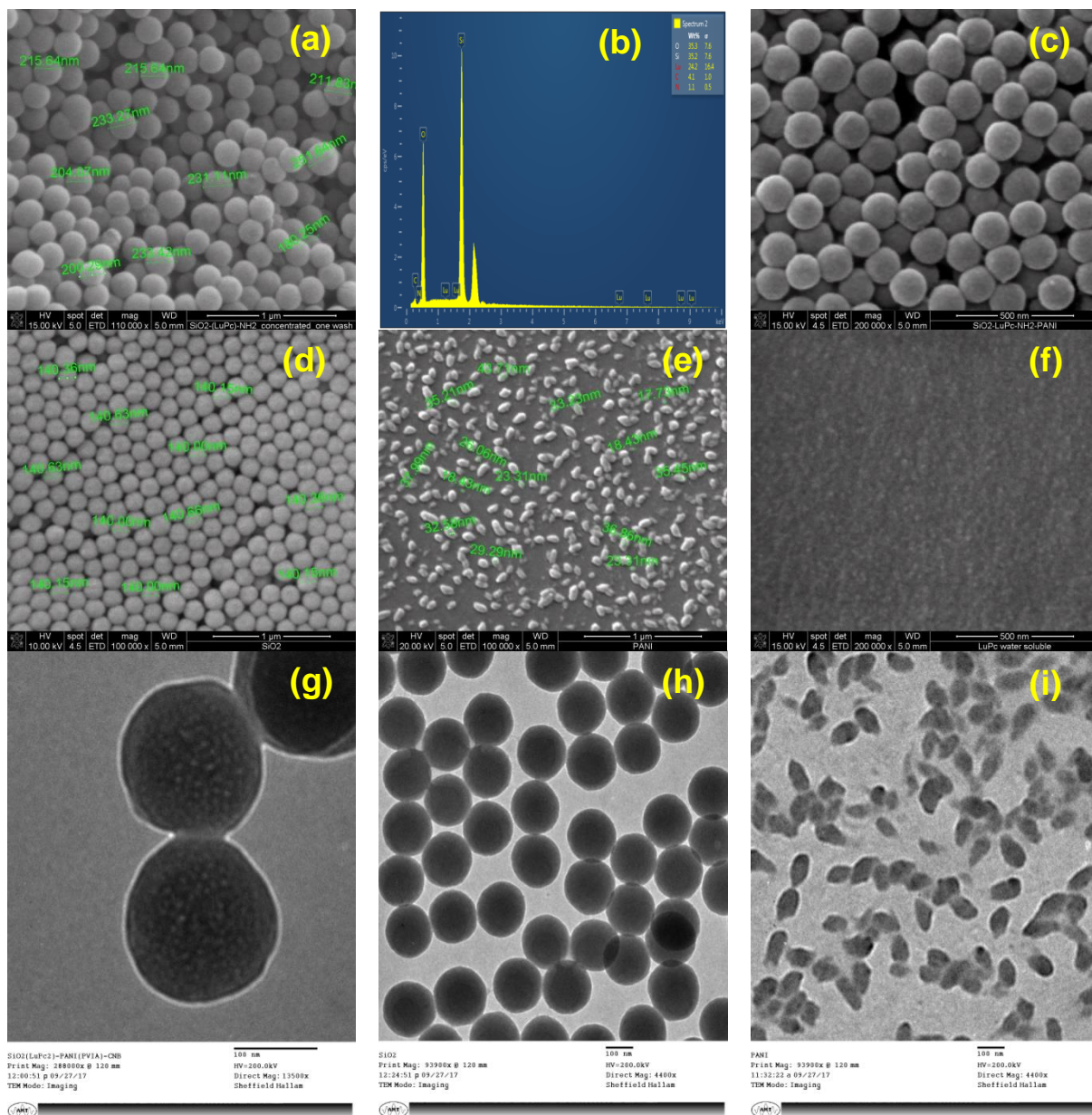


Fig. 1 SEM images of (a) $\text{SiO}_2(\text{LuPc}_2)$, (b) EDX image of $\text{SiO}_2(\text{LuPc}_2)$, (c) $\text{SiO}_2(\text{LuPc}_2)\text{-PANI(PVIA)-CNB}$, (d) SiO_2 , (e) PANI(PVIA), (f) LuPc_2 ; TEM images of (g) $\text{SiO}_2(\text{LuPc}_2)\text{-PANI(PVIA)-CNB}$, (h) SiO_2 , (i) PANI(PVIA)

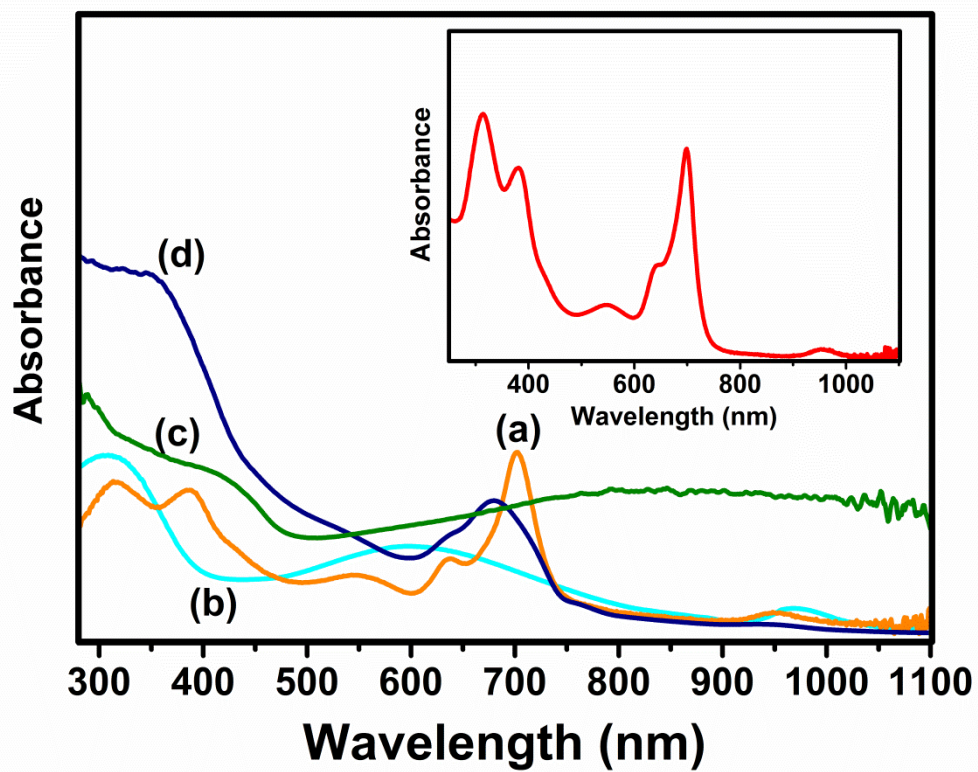


Fig. 2 UV-visible spectrum of (a) SiO₂(LuPc₂), (b) PANI-EB (dedoped), (c) PANI(PVIA), (d) SiO₂(LuPc₂)-PANI(PVIA)-CNB. Inset UV-visible spectrum of LuPc₂

1

2

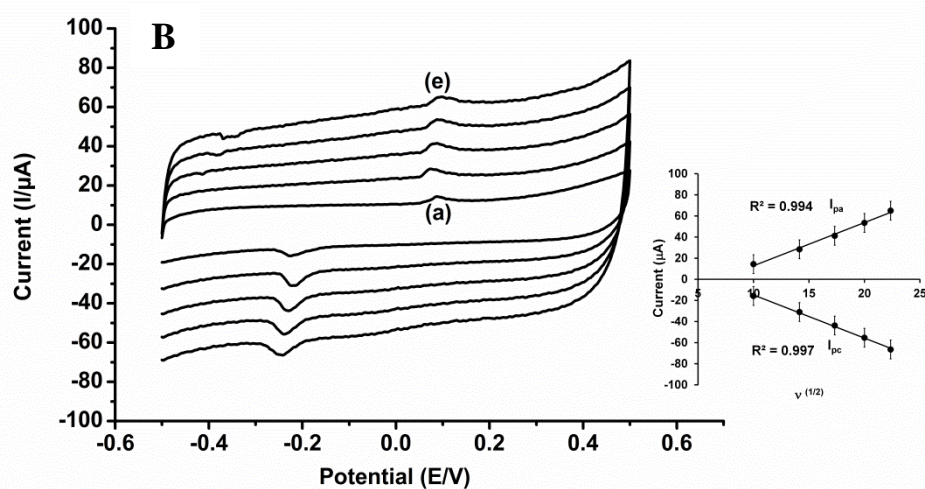
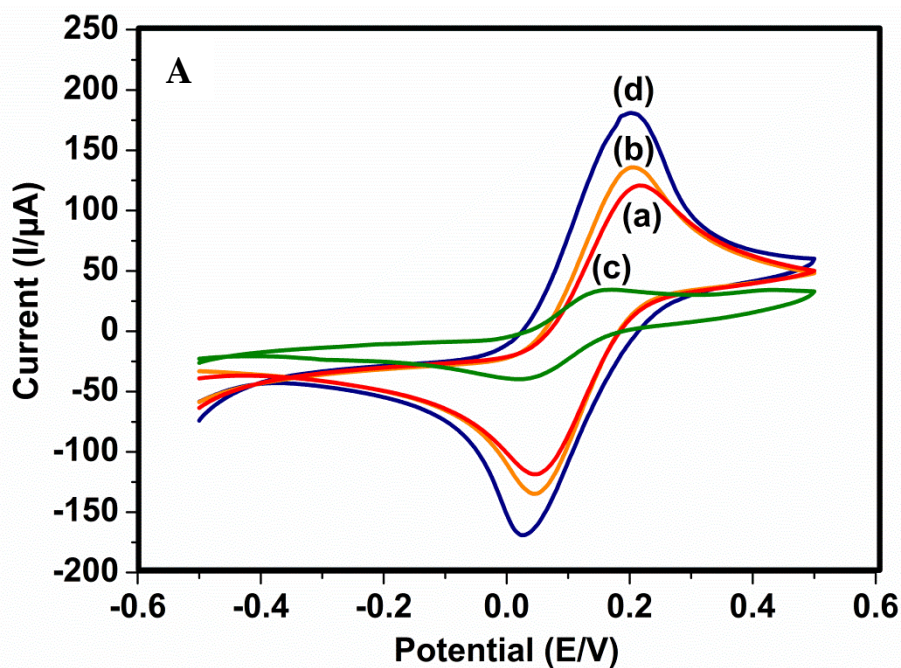


Fig. 3 (A) Cyclic voltammogram of (a) SiO_2 , (b) $\text{SiO}_2(\text{LuPc}_2)$, (c) PANI(PVIA) , (d) $\text{SiO}_2(\text{LuPc}_2)\text{-PANI(PVIA)-CNB}$ recorded in 5 mM Potassium ferro/ferri cyanide solution containing 0.1 M NaCl; scan rate = 100 mV/s (B) Cyclic voltammogram of $\text{SiO}_2(\text{LuPc}_2)\text{-PANI(PVIA)/GOx-CNB}$ in N_2 saturated 0.1 M PBS (pH 7.0) containing 0.1 M NaCl for different scan rate 100-500 mV/s (a-e); inset: plot of $v^{1/2}$ vs I_p

1

2

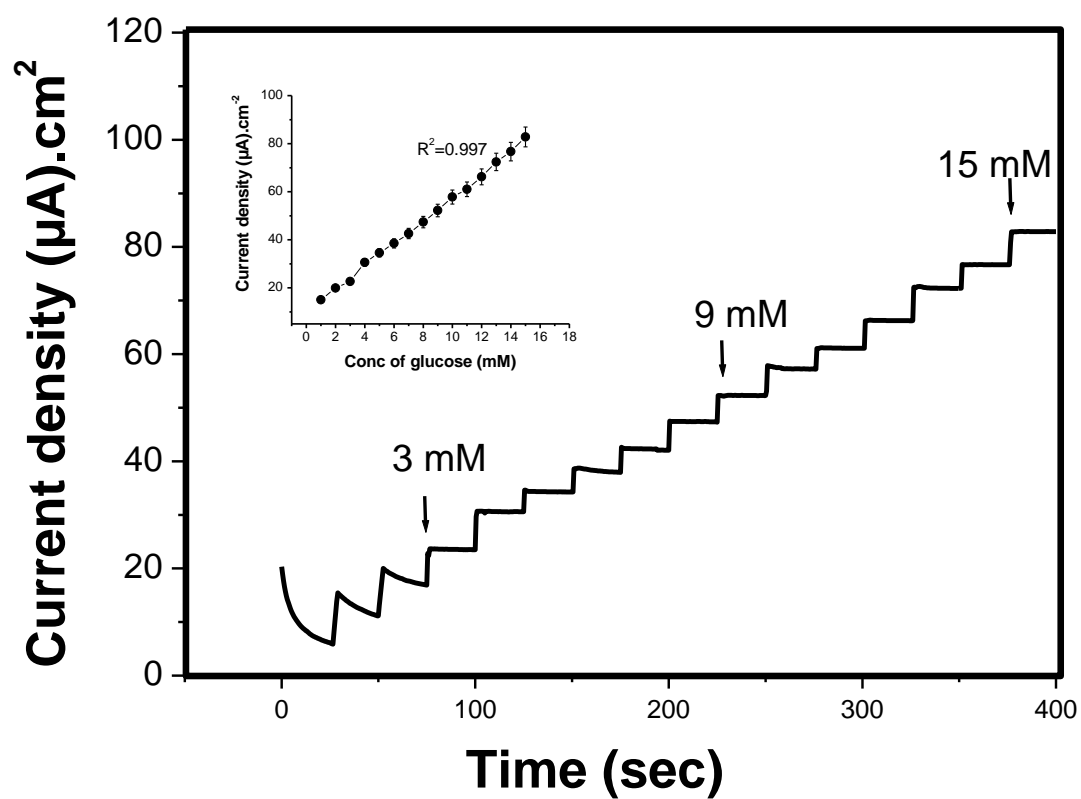


Fig. 4 Amperometry response for successive addition of glucose in 0.1 M PBS (pH 7.0) at $\text{SiO}_2(\text{LuPc}_2)\text{-PANI(PVIA)/GOx-CNB}$. Inset: calibration plot [glucose] vs peak current density